Research Article

Chemical Review and Letters
journal homepage: www.chemrevlett.com
ISSN (online): 2645-4947 (print) 2676-7279

Synthesis, characterization, DFT and biological studies mixed ligand metal complexes containing of a new Schiff base ligand and 2-aminopropane-1,3-diol

Akar Mahmood Muhammed[1,*], Eman Ibraheem Abdulkareem[2]

[1]*Chemistry Department, College of Science, University of Raparin, Rania, 46012, Sulaymaniyah, Iraq.*
[2]*Department of Chemistry, Faculty of Science and Health, Koya University, Danielle Mitterrand Boulevard, Koya KOY45, Kurdistan Region - F.R. Iraq.*

ARTICLE INFO

Article history:
Received 27 March 2025
Received in revised form 31 May 2025
Accepted 07 June 2025

Keywords:
Schiff base ligand
Mixed-ligand complexes
2-amino-3,5-dibromobenzaldehyde
2-aminopropane-1,3-diol
DFT

ABSTRACT

The Schiff base ligand (Z)-2-((2-amino-3,5-dibromobenzylidene)amino)phenol, was synthesized through a condensation reaction between 2-amino-3,5-dibromobenzaldehyde and 2-aminophenol in a 1:1 molar ratio. The structure of the ligand was confirmed and characterized by using various spectroscopic techniques including FT-IR, UV-visible, ^{1}H and ^{13}C-NMR spectroscopy, electron ionization mass spectrometry (EI-MS) and supported by DFT-optimized structures. The melting point of the compound was also determined. The metal complexes were synthesized by the reacting of Schiff base ligand with Ni(II), Mn(II), Cu(II) and Co(II) ions in 2:1 ligand-to-metal molar ratio. The resulting complexes have the general formulas $[M(L)(C_3H_7NO_2)]$ where M = Ni(II), Mn(II) and Cu(II) and $[Co(L)_2]$ for the cobalt complex, where $C_3H_7NO_2$ represents 2-aminopropane-1,3-diol. The complexes were characterized by FT-IR, UV-visible, molar conductance, magnetic moment measurements and melting point. The low molar conductance values indicate a non-electrolytic nature, while magnetic moment data confirm a tetrahedral geometry around all metal centers Ni(II), Mn(II), Cu(II) and Co(II). Furthermore, Antibacterial activity was evaluated by inhibition zone measurement. The ligand and its complexes were tested against Staphylococcus aureus and Pseudomonas aeruginosa, as a result complexes Mn(II) and Cu(II) showed antibacterial activity . Finally, the DFT studies assisted to better understand of the electronics structure, reactivity and stability of ligands.

1. Introduction

Schiff base ligands, first described by Hugo Schiff in 1864 are a class of chemical compounds characterized by the azomethine (-C=N-) functional group, which is formed through the condensation of the primary amines with carbonyl compounds [1].

A Schiff base is produced when the carbonyl group (C=O) of a ketone or aldehyde is replaced by an imine (-C=N-) functional group [2]. This functional group is essential in the coordination properties of Schiff bases with metallic ions, resulting in the production of strong metal complexes utilized in medicinal chemistry [3], catalysis, solar energy production and materials research [4].

Salicylaldimine-based Schiff bases which contain nitrogen and oxygen donor atoms, demonstrate significant coordination capacity with transition metals, hence improving their stability and bioactivity [5, 6].

The incorporation of halogen substituents such as bromine into the ligand structure can further adjust electrical characteristics, affect reactivity and enhance biological activity [7].

2-Aminophenol (C_6H_7NO) is an aromatic chemical characterized by the presence of an amino ($-NH_2$) and a hydroxyl (-OH) group bonded to a benzene ring in the ortho position, this dual-functional molecule is extensively employed as an intermediate in the manufacture of pigments, medicines and agrochemicals [8].

Owing to its coordinating capacity 2-aminophenol serves as a significant precursor in the synthesis of Schiff base Ligands and metallic complexes which demonstrate a diversity of biological and catalytic functions [9].

The bifunctional donor characteristics of 2-

* Corresponding author E-mail: akar.mahmood@uor.edu.krd
https://doi.org/10.22034/crl.2025.514151.1569

aminophenol including both nitrogen and oxygen donor sites, augment its chelating capacity rendering it an exemplary option for coordination chemistry [10]. 2-Amino-3,5-dibromobenzaldehyde is an aromatic molecule characterized by an amino group (-NH_2) and an aldehyde group (-CHO) on a benzene ring which is substituted with two bromine atoms at the 3 and 5 positions. This molecule functions as a multifaceted intermediate in the synthesis of Schiff bases which are widely researched for their chemical coordination and biological applications [11]. A presence of E-withdrawing bromine substituents increases the electrophilicity of the aldehyde group, hence promoting condensation processes with amines [12]. Furthermore, halogen atoms also enhance lipophilicity and possible bioactivity rendering it a significant precursor in the synthesis of metal complexes and bioactive compounds [13].

2-Aminopropane-1,3-diol is commonly referred to as serinol, is a bifunctional chemical molecule that possesses both amine and diol functional groups. The molecular structure ($C_3H_9NO_2$) features a core amino propane backbone with hydroxyl groups at the 1 and 3 positions which enhance its hydrophilic properties and reactivity [14]. This chemical is extensively utilized as a precursor in the manufacture of physiologically active compounds, encompassing medicines, surfactants and polymers. Owing to its chelating properties and ability to create stable coordination complexes 2-aminopropane-1,3-diol is significant in the advancement of metal-based medicinal medicines and coordination chemistry research [15]. The novelty of this study lies in the synthesis of a new bromine-substituted Schiff base ligand and its mixed-ligand complexes incorporating 2-aminopropane-1,3-diol, a rarely reported co-ligand. The work combines experimental characterization with DFT analysis to reveal structural, electronic and stability features. Notably, the Mn(II) and Cu(II) complexes exhibited significant antibacterial activity, highlighting potential biomedical applications and underscoring the importance of this research in coordination and bioinorganic chemistry. Scheme 1, illustrates the synthesis pathway of the Schiff base ligand and its metal complexes.

2. Materials and Methods

2.1. Material and instrumentation

All chemicals, including 2-aminophenol, 2-amino-3,5-dibromobenzaldehyde, glacial acetic acid, DMF, ethanol, and 2-aminopropane-1,3-diol, were purchased from commercial suppliers and used without further purification. Metal salts such as ($NiCl_2·6H_2O$, $MnCl_2.4H_2O$, $CuCl_2·2H_2O$, and $CoCl_2·6H_2O$) were also used as received. All solvents were dehydrated immediately prior to use.

Melting points were determined using a Stuart melting point apparatus, model ST15 OSA, with a standard power of 75 W. The FT-IR spectra were recorded using a Shimadzu IR Affinity-1 spectrophotometer in the range of 4000–400 cm^{-1}, using the KBr pellet method. The electronic spectra of the ligand and its metal complexes were recorded using a JENWAY 6705 UV-Visible spectrophotometer in the range of 200–900 nm, employing quartz cells with a path length of 1.0 cm and a concentration of 10^{-3} M in DMF. Molar conductance measurements were carried out using a Systronics-305 conductivity meter. Elemental (C, H, N) analyses were performed using a CHN analyzer. ^{1}H NMR spectra were recorded using a Bruker Advance 111, 400 MHz spectrometer. ^{13}C NMR spectra were obtained at 100 MHz and Magnetic susceptibility measurements were conducted at room temperature, adhering to Faraday's methodology. Magnetic moments were quantified using a magnetic susceptibility balanced (Johnson Matthey Catalyst System Div.). The mass spectrum of the ligand was recorded using electron impact ionization on a (Shimadzu GCMSQPA 1000).

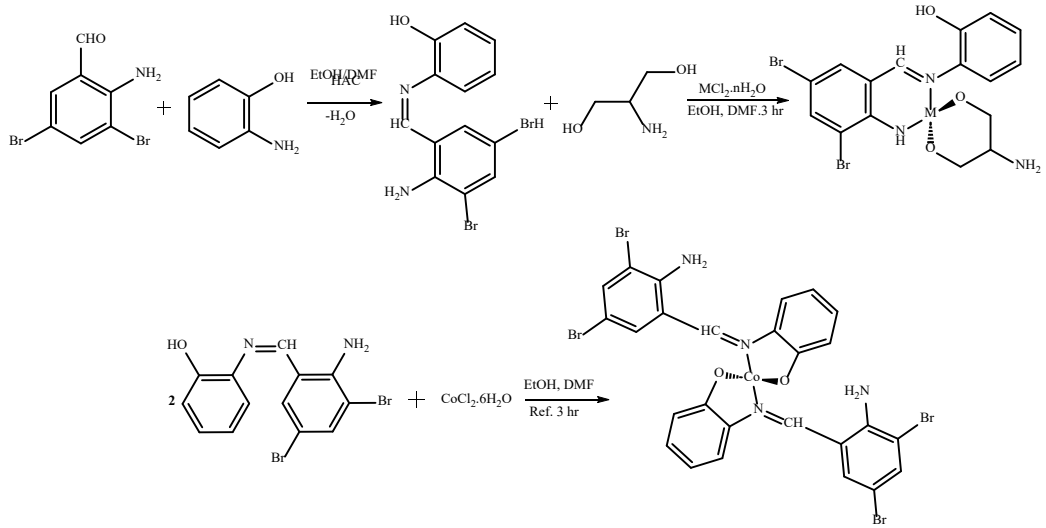

Scheme 1. Synthetic route of the ligand and its complexes where M= Ni(II), Mn(II) and Cu(II).

2.2. Synthesis of the ligand

The Schiff base ligand (Z)-2-((2-amino-3,5-dibromobenzylidene)amino)phenol, was synthesized by the condensation of equimolar amounts of 2-amino-3,5-dibromobenzaldehyde (2 g, 7.17 mmol) and 2-aminophenol (0.782 g, 7.16 mmol) in a mixed solvent of ethanol (15 ml) and DMF (5 ml). A few drops (3-4) of glacial acetic acid were added as a catalyst and the mixture was refluxed at 90 °C for 6 hours. The resulting precipitate was filtered, recrystallized from ethanol, and dried under vacuum, Yield: 78.5%; melting point: 152 °C. as illustrated in Scheme 1.

2.3. Syntheses of [Ni(L)($C_3H_7NO_2$)] mixed ligand complex

The mixed ligand complex was synthesized by dissolving the reactants in a solvent mixture of ethanol and dimethylformamide (DMF) at a 2:1 (v/v) ratio, utilizing 7 ml of ethanol and 3 ml of DMF. To this solution, (0.37 g ,1 mmol) of the Schiff base ligand, (0.09 g, 1 mmol) of 2-aminopropane-1,3-diol and (0.237 g, 0.997 mmol) of nickel (II) chloride hexahydrate ($NiCl_2 \cdot 6H_2O$) were added in a 1:1:1 molar ratio (L:M: diol), where diol denotes 2-aminopropane-1,3-diol. The mixture was subsequently heated under reflux at 80 °C for three hours, the resultant precipitate was flirted of, recrystallized with ethanol and dried under vacuum. Yield: 84%; melting point: 280 °C. As shown in Scheme 1.

2.4. Syntheses of [Mn(L)($C_3H_7NO_2$)] and [Cu(L)($C_3H_7NO_2$)] mixed ligan complexes

The same synthetic method employed for the synthesis of [Ni(L)($C_3H_7NO_2$)] was used to produce [Mn(L)($C_3H_7NO_2$)] and [Cu(L)($C_3H_7NO_2$)], resulting in dark brown and black colored complexes, respectively. As demonstrated in Scheme 1.

2.5. Syntheses of [$Co(L)_2$]

The complex was formed by reacting $CoCl_2 \cdot 6H_2O$ (0.237 g, 1 mmol) with two equivalents of the ligand (0.74 g, 2 mmol) in a mixed solvent of ethanol and DMF (15 ml).

The reaction mixture, exhibiting a metal-to-ligand molar ratio of 1:2, was refluxed for three hours. The resultant precipitate was filtered, rinsed, and dehydrated under vacuum conditions. Yield: 62%; melting point: 154 °C. As depicted in Scheme 1.

The physical properties of the ligand and its metal complexes are summarized in Table 1.

3. Results and Discussion

3.1. FT-IR spectra of the ligand and its complexes

The FT-IR spectra of the starting materials, the ligand and its metal complexes are presented in the supplementary section, the spectral data are summarized in Table 2. In the spectrum of 2-aminophenol (Fig. 1 Supp.), the bands observed in the range of (3373-3302 cm^{-1}) are assigned to the υ(N-H) stretching vibrations of the (-NH_2) primary amine group [16]. These bands are absent in the spectrum of the Schiff base ligand, indicating the reaction of 2-aminophenol with 2-amino-3,5-dibromobenzaldehyde. The spectrum of 2-amino-3,5-dibromobenzaldehyde (Fig. 2 Supp.), shows a strong band at (1660 cm^{-1}) attributed to the υ(C=O) stretching vibration of the aldehyde group, which appears at a lower frequency than that of typical aldehydes due to conjugation with the aromatic ring [17]. In the spectrum of the Schiff base ligand (Fig. 3 Supp.), the absence of the υ(C=O) band and the appears of a new band at (1618 cm^{-1}) υ(C=N) confirm the formation of the imine group through condensation.

The FT-IR spectra of all metal complexes Ni(II), Mn(II), Cu(II) and Co(II) are shown in (Fig. 4-8 Supp.), respectively. The υ(C=N) band is shifts to higher frequencies in the range (1660-1641 cm^{-1}), indicating coordination of the imine nitrogen to the metal center [2].

In the synthesis of mixed ligand complexes Ni(II), Mn(II) and Cu(II), 2-aminopropane-1,3-diol is utilized as a secondary ligand.

Table 1. The physical properties of the ligand and its complexes.

No.	Compounds	Chemical formula	M.wt	Yield %	Color	M.P. °C	Found/calculated		
							C	H	N
1.	Ligand	$C_{13}H_{10}Br_2N_2O$	370.04	78.5	yellow	152	42	2.90	7.80
							42.20	2.72	7.57
2.	[Ni(L)($C_3H_7NO_2$)]	$C_{16}H_{16}Br_2N_3NiO_3$	516.82	84	Light Brown	280	37.40	3.35	8.33
							37.18	3.12	8.13
3.	[Mn(L)($C_3H_7NO_2$)]	$C_{16}H_{16}Br_2MnN_3O_3$	513.06	67	Dark brawn	106	37.8	3.35	8.40
							37.46	3.14	8.19
4.	[Cu(L)($C_3H_7NO_2$)]	$C_{16}H_{16}Br_2CuN_3O_3$	521.67	56	black	246	37.2	3.3	8.23
							36.84	3.09	8.05
5.	[$Co(L)_2$]	$C_{26}H_{18}Br_4CoN_4O_2$	797.00	62	pink	154	39.44	2.52	7.22
							39.18	2.28	7.03

The FT-IR spectrum of 2-aminopropane-1,3-diol, (Fig. 4 Supp.), exhibits two absorption bands in the range of (3311-3269 cm^{-1}) corresponding to the υ(N-H) stretching vibration primary amine group [18, 19]. When coordinated with the metal these two bands are shifted to higher frequency at range (3360-3309 cm^{-1}). A broad band appearing at (3182 cm^{-1}) is attributed to the υ(O-H) stretching vibration [20, 21]. This band disappeared in the spectra of mix ligand complexes Ni(II), Mn(II) and Cu(II) due to interaction with the metal center and complex formation. Additionally, a band appears in the spectra of the mixed ligand complexes of Ni(II), Mn(II) and Cu(II) at (3262, 3317 and 3219 cm^{-1}) respectively, corresponding to the υ(N-H) stretching of a secondary amine [22]. This signifies the coordination of the ($-NH_2$) group to the metal center. The bands at the range of (484-420 cm^{-1}) are due to υ(M-N) stretching vibrations [23]. while υ(M-O) stretching vibrations are observed between (570-510 cm^{-1}) [24].

3.2. **UV-visible spectrum of the ligand and its Complexes**

The electronic spectra of the ligand and its metal complexes are illustrated in the Figure 1(a-e). A summary of the corresponding absorption peaks for the ligand and its complexes is provided in Table 3. The UV-visible spectrum of the ligand Figure 1(a), exhibit two peaks, a strong peaks at (271 nm) (36900 cm^{-1}, ε_{max}= 2608 dm^3 mol^{-1} cm^{-1}) and (393 nm) (25445 cm^{-1}, ε_{max}= 2451 dm^3 mol^{-1} cm^{-1}), the band at (271 nm) is assigned to ($\pi\rightarrow\pi^*$) benzene ring [25] , a band at (393 nm) results from the ($n\rightarrow\pi^*$) transition non-bonding electron on nitrogen imine group (-HC=N) and transition of the phenolic group [26]. In the spectrum of the Ni(II) complex, four absorption bands are observed, as shown in Figure 1(b). A strong band appears at (216 nm) (46,296 cm^{-1}, ε_{max} = 1262 dm^3 mol^{-1} cm^{-1}), attributed to a ($\pi\rightarrow\pi^*$) transition [27]. A shoulder peak is observed at (242 nm) (41,322 cm^{-1}, ε_{max} = 1094 dm^3 mol^{-1} cm^{-1}), corresponding to an ($n\rightarrow\pi^*$) transition [28]. A weak band at (420 nm) (23,809 cm^{-1}, ε_{max} = 377 dm^3 mol^{-1} cm^{-1}) is assigned to a ligand-to-metal charge transfer (LMCT) transition [29]. Another band at (516 nm) (19,493 cm^{-1}, ε_{max} = 298 dm^3 mol^{-1} cm^{-1}) is attributed to a d-d transition of ($^3T_{1(F)}\longrightarrow{}^3T_{2(P)}$) supporting a tetrahedral geometry around the Ni(II) ion [30]. The UV-visible spectrum of the Mn(II) complex, as shown in Figure 1(c), exhibits four absorption bands. A strong band at (217 nm) is attributed to an intra-ligand ($\pi\rightarrow\pi^*$) transition, while a weak band at (238 nm) corresponds to an ($n\rightarrow\pi^*$) transition.

Table 2. FT-IR spectral data of the ligand and its complexes.

No.	Compounds	υ(NH_2)	υ(O-H)	υ(C=O)	υ(C=N)	υ (M-O)	υ(M-N)
A.	2-aminophenole	3373-3302	3051	-	-	-	-
B.	2-amino-3,5-dibromobenzaldehyde	3450-3250	-	1680	-	-	-
1.	Ligand	3372-3334	3448	-	1618	-	-
2.	2-aminopropane-1,3-diol	3311-3269	3182	-	-	-	-
3.	[Ni(L)($C_3H_7NO_2$)]	3334-3309	3110	-	1658	512 m	423 w
4.	[Mn(L)($C_3H_7NO_2$)]	3462-3446	3217	-	1643	549 m	464 w
5.	[Cu(L)($C_3H_7NO_2$)]	3460-3446	3219	-	1641	557 w	437 m
6.	[$Co(L)_2$]	3446-3332	-	-	1660	549 m	484 m

m = medium, w = weak

Table 3. The electronic spectral data of the ligand and its metal complexes.

No.	Compounds	Band Position (λ nm)	Electronic transition (cm^{-1})	ε_{max} ($dm^3mol^{-1}cm^{-1}$)	Assignment	Suggested configuration
1.	Ligand	271	36900	2608	$\pi\rightarrow\pi^*$	-
		393	25445	2451	$n\rightarrow\pi^*$	
2.	[Ni(L)($C_3H_7NO_2$)]	216	46296	1262	$\pi\rightarrow\pi^*$	Tetrahedral
		242	41322	1094	$\pi\rightarrow\pi^*$	
		420	23809	377	C.T	
		516	19379	298	$^3T_{1(F)}\longrightarrow{}^3T_{2(P)}$	
3.	[Mn(L)($C_3H_7NO_2$)]	217	46082	1187	$\pi\rightarrow\pi^*$	Tetrahedral
		238	42016	951	$n\rightarrow\pi^*$	
		389	25706	230	C.T	
		513	19493	93	$^6A_1\rightarrow{}^4T_{1(G)}$	
4.	[Cu(L)($C_3H_7NO_2$)]	219	45662	1659	$\pi\rightarrow\pi^*$	Tetrahedral
		238	42016	1553	$n\rightarrow\pi^*$	
		443	22573	757	C.T	
		503	19880	775	$^3T_{1(P)}\rightarrow{}^3T_{1(F)}$	
5.	[$Co(L)_2$]	235	42553	1813	$\pi\rightarrow\pi^*$	Tetrahedral
		413	24213	611	$^4A_2\rightarrow{}^4T_{1(P)}$	
		550	18181	250	$^4A\rightarrow{}^4T_{1(F)}$	

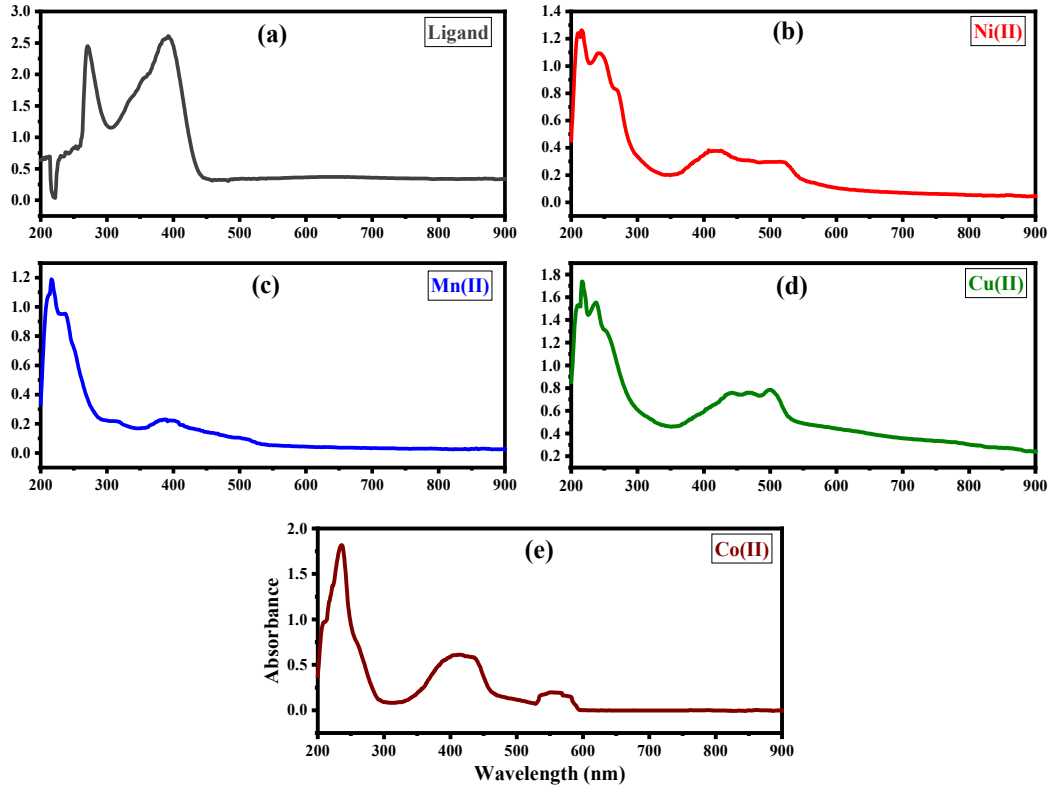

Fig. 1. (a) UV-visible spectrum of the free ligand, (b) UV-visible spectrum of the Ni(II) complex, (c) UV-visible spectrum of the Mn(II) complex, (d) UV-visible spectrum of the Cu(II) complex and (e) UV-visible spectrum of the Co(II) complex.

The band observed at (389 nm) is assigned to a (LMCT) transition [31]. Additionally, a weak band at (513 nm) is assigned to the spin-forbidden ($^6A_1 \rightarrow {}^4T_{1(G)}$) d-d transition, consistent with a tetrahedral Mn(II) complex [32]. In the spectrum of the Cu(II)) complex Figure 1(d), Displayed four absorption bands at (219, 238, 443 and 503 nm). The bands at (219 nm) and (238 nm) are attributed to intra-ligand transitions. The absorption band at (443 nm) is assigned to (LMCT) transition [33], while the weak broad band at (503 nm) corresponds to a d-d transition ($^3T_{1(P)} \rightarrow {}^3T_{1(F)}$), indicating a tetrahedral geometry [34]. In the UV-visible spectrum of the Co(II) complex Figure 1(e), three absorption bands were observed. A strong band at (235 nm) is attributed to ($\pi \rightarrow \pi^*$) transition ligand, while a shoulder band at (413 nm) is assigned to a (LMCT) transition ($^4A_2 \rightarrow {}^4T_{1(P)}$). A weak band at (531 nm) is attributed to a d-d transition metal ion for ($^4A \rightarrow {}^4T_{1(F)}$)of the Co(II) ion, confirmed the tetrahedral geometry of the complex [35].

3.3. **Conductivity Measurements**

The molar conductivity values of the metal ion complexes in DMF (10^{-3} M) were measured at room temperature. As shown in Table 4. The recorded conductance values were all below (11 $\Omega^{-1}\cdot cm^2\cdot mol^{-1}$) indicating that the synthesized complexes exhibit non-electrolytic behavior [36]. This suggests the absence of ionic species outside the coordination sphere of the complexes.

3.4. **Magnetic susceptibility**

The magnetic moment of the complexes determined using Faraday's method, provides insight into the coordination geometry of the metal ions. The magnetic susceptibility measurements were carried out using a Gouy balance, allowing for the estimation of the number of unpaired electrons in each complex [37]. Table *5* presents the results of the effective magnetic moment (μ_{eff} = B.M) determined from the magnetic susceptibility measurements of selected complexes at room temperature. By utilizing the equation (μ_{eff} = 2.828 X$\sqrt{}$ AT), the estimated (μ_{eff}) indicates all complexes exhibit high spin characteristics. The electron configurations of the d-orbitals for the metal ions are as follows: Ni(II) has 2 unpaired and 3 paired electrons, Mn(II) has 5 unpaired electrons, Cu(II) has 1 unpaired and 4 paired electrons, and Co(II) has 3 unpaired and 2 paired electrons. These configurations support sp^3 hybridization, signifying a tetrahedral geometry for all complexes.

3.5. ^{1}**H-NMR Spectroscopy**

The ^{1}H-NMR spectrum of the ligand in DMSO-d_6 (Fig. 9 Supp.), displays a singlet at δ (8.70 ppm), corresponding to the azomethine proton CH=N- of the Schiff base. Another singlet at δ (9.43 ppm) is attributed to the phenolic -OH proton [38]. Multiple signals appearing in the range of δ (6.83-7.75 ppm) correspond to the six aromatic protons [39]. In contrast, a singlet at δ

(3.43 ppm) is attributed to the amine -NH_2 protons, while the peak at δ (2.45 ppm) corresponds to the residual DMSO solvent [40]. The spectral data are listed in Table 6.

3.6. ^{13}C-NMR Spectroscopy

The ^{13}C-NMR spectra further substantiate the structural characterization of the ligand, is shown in (Fig. 10 Supp.) and the corresponding data summarized in Table 7. The signals reflect magnetically non-equivalent carbon atoms. The ^{13}C-NMR spectrum of the ligand shows a signal at δ (160.77 ppm) attributed to the azomethine carbon CH=N-. Two signals at δ (105.00 and 116.87 ppm) correspond to the aromatic carbons bearing bromine C-Br, while the signal at δ (151.33 ppm) is assigned to the phenolic carbon C-OH. In addition, a signal at δ (145.71 ppm) corresponds to the C-NH_2 carbon within the aromatic ring. The peaks at δ (138.34, 120.00 ppm) are assigned to the C-N and C-CH=N groups of the benzene ring, respectively. Six signals in the range δ (109.75-136.13 ppm) are attributed to aromatic C=C carbons [41]. Furthermore, five peaks observed around δ (40 ppm) correspond to the DMSO solvent [42].

3.7. Mass Spectrum of the ligand

The mass spectrum of the ligand is displayed in (Fig. 11 Supp.). A molecular ion peak was observed at (370.1 m/z) which corresponding to the Schiff base ligand moiety $[C_{13}H_9Br_2N_2O]^+$, calculated molecular weight (371.04 g/mol). Additional peaks at (288, 209.1, 179, 104, and 77 m/z) correspond to stable fragment ions, supporting the successful synthesis and purity of the ligand. The observed fragments are summarized in Table 8.

Table 4. Molar conductivity data of the synthesized metal complexes.

Complexes	Chemical formula	Molar conductance ($\Omega^{-1}\cdot cm^2\cdot mol^{-1}$)	Behavior
$[Ni(L)(C_3H_7NO_2)]$	$C_{16}H_{16}Br_2N_3NiO_3$	7.6	Non-electrolyte
$[Mn(L)(C_3H_7NO_2)]$	$C_{16}H_{16}Br_2MnN_3O_3$	10	Non-electrolyte
$[Cu(L)(C_3H_7NO_2)]$	$C_{16}H_{16}Br_2CuN_3O_3$	3.5	Non-electrolyte
$[Co(L)_2]$	$C_{26}H_{18}Br_4CoN_4O_2$	5.85	Non-electrolyte

Table 5. Magnetic moment data (μ_{eff} = B. M) at 298 K for the synthesized complexes.

Complexes	$X_g \times 10^{-6}$ gram susceptibility	$X_m \times 10^{-3}$ molar susceptibility	$X_A \times 10^{-3}$ atom susceptibility	μ_{eff} (M.B) Expt.	μ_{eff} (B.M) Calc.	Proposed structure
$[Ni(L)(C_3H_7NO_2)]$	7.43	3.84	3.62	2.8-4	2.94	Tetrahedral
$[Mn(L)(C_3H_7NO_2)]$	27	13.9	13.7	5.9-6.2	5.72	Tetrahedral
$[Cu(L)(C_3H_7NO_2)]$	3	1.58	1.36	1.7-2.2	1.8	Tetrahedral
$[Co(L)_2]$	12.7	10.2	9.9	4.5-5	4.86	Tetrahedral

Table 6. ^{1}H-NMR spectral data of the ligand.

Hydrogen No.	Group	δ (ppm)
1(CH=N) singlet.	Azomethine	8.70
1(OH) singlet.	Phenolic	9.43
6(H Aromatic) multiple	Ring	6.83-7.75
(NH_2) singlet.	Amine	3.43
DMSO	-	2.45

Table 7. ^{13}C-NMR spectral data of the ligand.

Carbon No.	Group	δ (ppm)
1(CH=N)	Imine	160.77
2(C-Br)	Benzene ring	105-116.87
1(C-OH)	phenolic	151.33
1(C-NH_2)	Benzene	145.71
1(C-N)	Benzene	138.34
1(C-CH=N)	Benzene	120
6(C=C)	Benzene ring	109.75-136.13
DMSO	-	40

Table 8. Mass spectral data of the ligand.

Fragmentations	Mass/charge(m/z)	Relative abundance
$[C_{13}H_9Br_2N_2O]^+$	370.1	100
$[C_{13}H_{10}BrN_2O]^+$	288	10.0
$[C_{13}H_9N_2O]^+$	209.1	9.2
$[C_{13}H_9N]^+$	179	8.9
$[C_7H_6N]^+$	104	7.5
$[C_6H_5]^+$	77	19.8

3.8. Biological activity of the ligand and its complexes

The biological activity of the ligand and its complexes Ni(II), Mn(II), Cu(II) and Co(II), was tested against two kinds of harmful bacteria. utilizing the inhibition method [43]. The two bacterial kinds were Gram-positive Staphylococcus aureus and Gram-negative pseudomonas aeruginosa [4, 44]. The ligand and Ni(II) complex did not exhibit any inhibitory activity against either bacterial strain after 24 hours, as shown in Figure 2. In contrast, the Mn(II) and Cu(II) complexes displayed zones of inhibition against both strains, indicating greater antibacterial activity compared to the ligand and Ni(II) complex. Additionally, the Co(II) complex showed an inhibitory zone against the Gram-positive Staphylococcus aureus but had no effect on the Gram-negative Pseudomonas aeruginosa. Norfloxacin at 30 µg is employed as a standard for both bacterial strains. The inhibitory zones were quantified in mm, and the results are presented in Table 9.

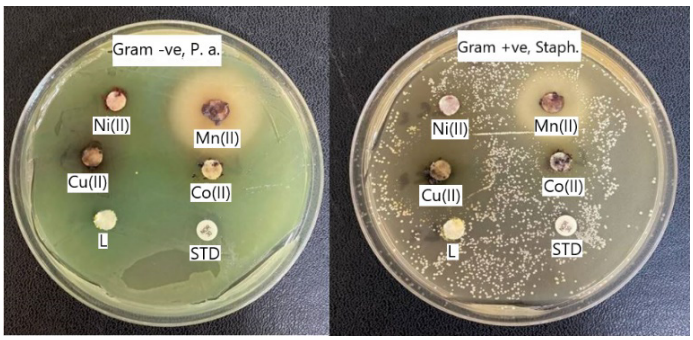

Fig. 2. The biological activity of ligand and their complexes.

3.9. Stability Measurement of the mixed-ligand Ni(II) Complex Using UV-visible Spectroscopy

The stability of the synthesized Ni(II) complex was evaluated over time using UV–visible spectroscopy. The absorbed spectra were documented at many distinct intervals. The UV-visible spectra remained unchanged across all experiments, indicating no significant shifts in absorption maxima or peak intensity. This consistency indicates that the Ni(II) complex maintains structural integrity and stability under the experimental conditions. The unchanged spectrum indicates the complex's stability making it suitable for coordination chemistry and biological applications [40]. The stability of the Ni(II) complex was evaluated by measuring its absorbance at several time points 24, 48, and 72 hours, as well as one, two, and three weeks. No significant changes in absorbance were detected, confirming its stability. The stability of the Ni(II) complex, as demonstrated by UV-visible spectroscopy, is illustrated in Figure 3.

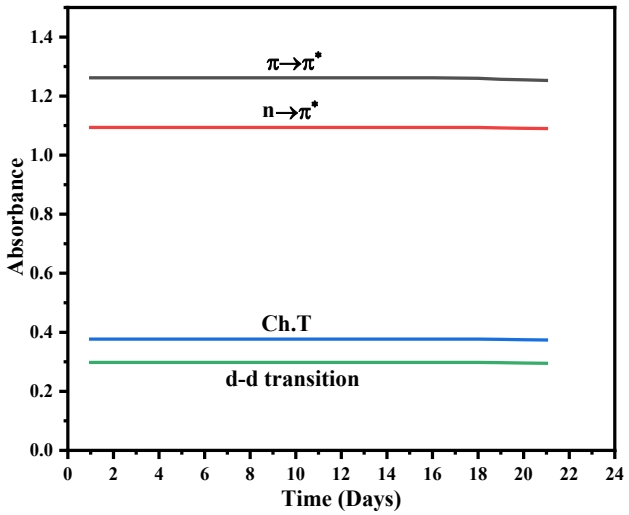

Fig. 3. The stability Ni(II) complex by UV-visible spectroscopy.

3.10. DFT-optimized Structures and HOMO-LUMO Energies of ligand

The HOMO, LUMO and global properties of the indicated molecule presents in Table 10. This data was acquired via the (LanL2DZ) basis set and the DFT/B3LYP theoretical framework [45, 46]. The energy gap denotes the disparity between a molecule's kinetic stability and its chemical reactivity, it including both EHOMO and ELUMO [47]. A molecule possessing a molecule with a substantial HOMO-LUMO gap is considered hard. Less soft, indicating a diminutive size and markedly diminished polarizability. Table 10 presents the calculated results based on the energy values of the HOMO and LUMO orbitals. The negative chemical potentials of (-5.7163 and -2.0629), respectively, show that these compounds are stable and do not decompose into their basic components. The HOMO-LUMO energy gap (ΔE = 3.6534 eV) with the (LanL2DZ) basis set is a crucial parameter that defines the molecule's reactivity and stability [48], with a larger gap signifying lower chemical reactivity and higher stability.

Table *9.* Antibacterial activity data of the ligand and its metal complexes.

No.	Compounds	Chemical formula	Zone of inhibition of samples (mm) in:	
			Gram (-Ve) pseudomonas aeruginosa	Gram (+Ve) Staphylococcus aureus
1.	Ligand	$C_{13}H_{10}Br_2N_2O$	-	-
2.	$[Ni(L)(C_3H_7NO_2)]$	$C_{16}H_{16}Br_2N_3NiO_3$	-	-
3.	$[Mn(L)(C_3H_7NO_2)]$	$C_{16}H_{16}Br_2MnN_3O_3$	15	16
4.	$[Cu(L)(C_3H_7NO_2)]$	$C_{16}H_{16}Br_2CuN_3O_3$	8	20
5.	$[Co(L)_2]$	$C_{26}H_{18}Br_4CoN_4O_2$	-	10

Table 10. The quantum chemical parameters of the ligand.

Parameters	Values
HOMO (eV)	-5.7163
LUMO (eV)	-2.0629
ΔE (eV)	3.6534
Ionization potential IP"(eV)	5.7163
Electron affinity "EA"(eV)	2.0629
Chemical hardness "η" (eV)	1.8267
Chemical softness "S" (eV^{-1})	0.5474
Electronegativity "χ" (eV)	3.8896
Chemical potential "μ"(eV)	-3.8896
Electrophilicity "ω" (eV)	4.1411
Nucleophilicity "Nu" (eV^{-1})	0.2415
ΔE backdonation	-0.4567
Transfer electron fraction ΔN	2.8407
Dipole-moment (Debye)	6.415632

The small energy gap with a (LanL2DZ) basis set indicates that this more flexible basis set can more effectively account for electron correlation, demonstrating significant electronic diffusion from donor to acceptor orbitals [49]. The literature research indicates that molecules with high ionization potential and chemical hardness exhibit low reactivity, while soft molecules are more reactive due to their greater electron transfer ability. The ionization potential (IP = 5.7163 eV) reflects the molecule's tendency to lose an electron (oxidation), while the electron affinity (EA = 2.0629 eV) indicates its tendency to gain an electron [50].

The chemical harshness (η = 1.8267 eV) indicates the molecule's barrier to alterations in electron density, with elevated values denoting enhanced stability, whereas chemical softness (S = 0.5474 eV^{-1}), its reciprocal, denotes heightened reactivity. A high Electronegativity (χ = 3.8896 eV) for (LanL2DZ) basis set indicates a molecule's capacity to attract electrons, hence affecting its interactions with adjacent entities. The electrophilicity index (ω = 4.1411 eV) measures the molecule's propensity for accepting electrons, which is essential for its reactivity [50]. The back-donation energy (ΔE = -0.4567 eV), and the transferred electrons (ΔN) exhibit positive values, (ΔN = 2.8407 eV), a positive ΔN indicates that the molecules are emitting electrons and signify electron transfer between the ligand and metal center, enhancing complex stability. A high dipole moment (6.42 Debye, LanL2DZ) indicates significant charge polarity within the molecule [51].

The Molecular Electrostatic Potential (MEP) map of the ligand explains its charge distribution and potential reactive sites. The MEP was calculated via the (DFT/LanL2DZ) basis set [52]. displaying areas with differing electrical potential. Figure 4. displays the Molecular Electrostatic Potential (MESP) surface of the ligand.

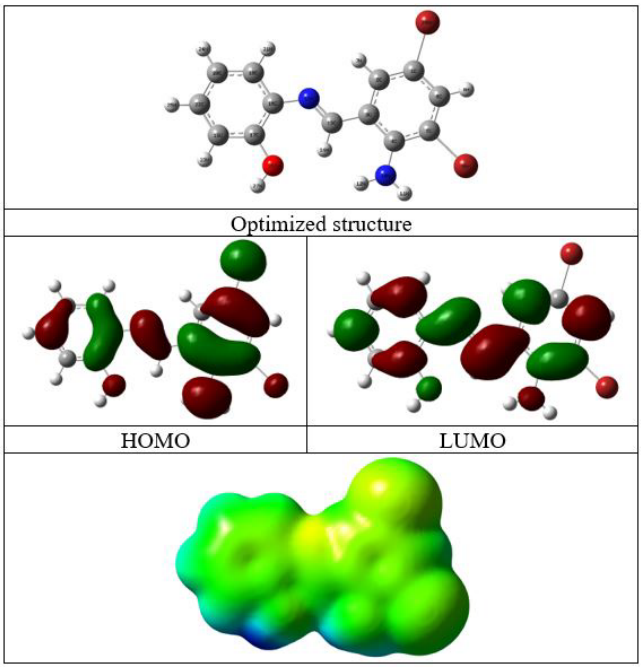

Fig. 4. The optimized structure, LUMO, HOMO and MEP for the ligand.

The predominantly green surface indicates a neutral electrostatic potential, reflecting a balanced electron density with no significant nucleophilic or electrophilic regions [5]. Small blue portions correspond to electron-deficient areas, potentially serving as electrophilic sites, whereas yellow regions signify electron-rich, nucleophilic sites [53]. The MEP analysis forecasts ligand-metal interactions and coordination, facilitating comprehension of chemical reactivity and biological activity.

4. Conclusion

The interaction between 2-aminophenol and 2-amino-3,5-dibromobenzaldehyde resulted in the synthesis of a novel Schiff base ligand. The reaction of this ligand with metal chlorides Ni(II), Mn(II), Cu(II), and Co(II) in the presence of 2-aminopropane-1,3-diol lead to the formation of tetrahedral metal complexes with the general formula $[M(L)(C_3H_7NO_2)]$, where M = Ni(II), Mn(II), and Cu(II). While Co(II) formed a distinct $[Co(L)_2]$ complex. Spectroscopic analyses confirmed complex formation, with FT-IR spectra showing characteristic shifts indicating ligand coordination. The UV-visible spectra showed distinct peaks in the visible region, confirming d-d transitions and metal ion coordination. Furthermore, the ^{1}H and ^{13}C-NMR analyses corroborated the structure of the Schiff base ligand. The nature of the fragments in the mass spectrum frequently elucidates the ligand's molecular structure. The Magnetic moment measurements supported the concluded geometrical shapes of all the complexes which is the tetrahedral. Conductivity measurements indicate that all complexes are non-electrolytic. Antibacterial studies revealed enhanced activity of Mn(II) and Cu(II) complexes over the free ligand, likely due to increased lipophilicity improving bacterial membrane interaction. The DFT-optimized structures indicate the HOMO-LUMO and all chemical and physical properties. MEP mapping delineates critical interaction sites for metal coordination and biological function. Finally, a novel bromine-substituted Schiff base and its metal complexes with 2-aminopropane-1,3-diol were synthesized and characterized. The Mn(II) and Cu(II) complexes showed notable antibacterial activity, indicating potential bioinorganic applications.

Supplementary files

Supplementary file 1.

Acknowledgements

I express my profound gratitude to my supervisor, Assist. Prof. Dr. Iman Ibrahim, for her guidance and encouragement. I also acknowledge the support of the Chemistry Department personnel at the University of Raparin in conducting the requisite measurements, also Many thanks for dear Assist prof. Dr. Rebaz Anwar Omer for helping me.

References

[1] T.Y. Fonkui, et al., Benzimidazole Schiff base derivatives: Synthesis, characterization and antimicrobial activity. *BMC Chem.*, 13 (2019) 1-11.

[2] A.M. Adelabu, et al., Synthesis, characterization and antimicrobial activity of a schiff base derived from 2-aminobenzothiazole with o-vanillin and its copper (II) complex. *Med. Med. Chem.*, 2 (2025) 141-145.

[3] D.K.T. Joshi, N.R.J.M. Pandya, M. Chemistry, Recent advances in microwave assisted synthesis of biological active 2-aminothiazole-schiff bases and their metal chelates. *Med. Med. Chem.*, 2 (2025) 123-128.

[4] D.J. Sakhare, Synthesis of Schiff Bases Ligand And Biological Activities of Their Transition Metal Complexes. *J. Chem. Technol.*, 1 (2025) 189-195.

[5] A. Mouna, et al., Spectroscopic analysis and theoretical comparison of the reactivity of 6-amino-3 (R) benzophenone reactions with acetylacetone. *Chem. Rev. Lett.*, 7 (2024) 942-956.

[6] R.K. Deo, C.J. Kumar, Synthesis and spectral characterization of binuclear compounds of Cu (II) and Ni (II) Schiff base of 2-Hydroxy-5-methylacetophenone and 1, 2-Propylenediamine with alkali metal salts of trinitrophenol. *J. Chem. Lett.*, 4 (2023) 81-85.

[7] A. Mamindla, et al., Comparative DNA-/BSA-binding, DNA cleavage, and cytotoxic properties of copper (II) amino/salicyl-phenolate Schiff bases (phen) complexes that induce generation of phenoxyl radicals. *Polyhedron*, 243 (2023) 116534.

[8] Z.Z. Chen, et al., An insight into the molecular structures, theoretical calculation and catalytic activities of novel heterotrinuclear [Cu II 2 Ce III] and heterohexanuclear [Cu II 4 Y III 2] bis (salamo)-based complexes. *New J. Chem.*, 44 (2020) 19836-19849.

[9] D.K. Kafi, A.N. Ayyash, A.S. Mohammed, Theoretical Study of Structural Properties and Energies of a 2-Aminophenol-Vanillin Molecule. *J. Phys. Conf. Ser.*, (2019) IOP Publishing.

[10] K. Savitha, S. Vedanayaki, Synthesis, spectral elucidation, antibacterial, antioxidant and DNA studies of ONNO tetradentate Schiff base metal (II) complexes derived from Benzene-1, 4-dicarboxaldehyde. (2021).

[11] S. Eğlence-Bakır, et al., Synthesis, molecular modelling, FT-IR, Raman and NMR characterization, molecular docking and ADMET study of new nickel (II) complex with an N4-tetradentate thiosemicarbazone. *J. Biomol. Struct. Dyn.*, 39 (2021) 4212-4224.

[12] B. Pinchaipat, et al., Synthesis, Characterization and Biological Studies of Nickel (Ii) and Zinc (Ii) Complexes with Mono-and Di-Bromo Substituted Schiff Base Ligands. *Available at SSRN 3698599*, (2020).

[13] K. Mohammadi, S.S. Azad, A. Amoozegar, New tetradentate Schiff bases of 2-amino-3, 5-dibromobenzaldehyde with aliphatic diamines and their metal complexes: Synthesis, characterization and thermal stability. *Spectrochim. Acta A*, 146 (2015) 221-227.

[14] E. Angelini, New Synthetic Strategies Involving Dearomatization. (2023).

[15] Y.V. Minnow, V.L. Schramm, Purine and pyrimidine pathways as antimalarial targets, in *Malaria-Recent Advances and New Perspectives*, (2022) IntechOpen.
[16] S.Q. Raji, A.T. Bader, Synthesis and Characterization of Ni (II) Schiff Base Complex as a Precursor for NiO Nanoparticles and an Investigation of Their Corrosion Inhibition. *Sci. Technol. Indones.*, 9 (2024).
[17] Q.C. Ran, Y. Gu, Concerted reactions of aldehyde groups during polymerization of an aldehyde-functional benzoxazine. *J. Polym. Sci. A*, 49 (2011) 1671-1677.
[18] M.N. Tawfeeq, S. Majeed, E. Al Samarrai, Synthsis, characterization and spectral estimation of Nickel (II), Copper (II) and their Complexes Activity as Antibacterial. *Chem. Rev. Lett.*, 7 (2024) 1031-1041.
[19] P.E. Omuku, et al., Preparation and characterization of yam peel biomass for decontamination of pollutants from hair-dressing saloon wastewater within Awka metropolis. *Med. Med. Chem.*, 2 (2025) 108-114.
[20] A.L. Negrete, R.V. Ramos, H.M.C. Beltran, Six-Membered Heterocyclic Boronate Esters. Synthesis and Structural Analysis. *J. Mex. Chem. Soc.*, (2023).
[21] J. Talat Mehrabad, F. Arjomandi Rad, E. Dargahi Maleki, Synthesis and characterization of Gabapentin-Zn2 Al-LDH nanohybrid and investigation of its drug release and biocompatibility properties on a laboratory scale. *J. Chem. Lett.*, 5 (2024) 71-78.
[22] N.A. Al-Mohammadi, A.S. Al-Fahdawi, S.S. Al-Janabi, Design and characterization of new dinuclear macrocyclic dithiocarbamate complexes by the preparation of a free ligand derived from isopropylamine. *Iraqi J. Sci.*, (2021) 1-15.
[23] H.A. El-Boraey, M.A. El-Salamony, A.A. Hathout, Macrocyclic [N 5] transition metal complexes: synthesis, characterization and biological activities. *J. Incl. Phenom. Macrocycl. Chem.*, 86 (2016) 153-166.
[24] E.N. Md Yusof, et al., Synthesis, characterization and biological evaluation of transition metal complexes derived from N, S bidentate ligands. *Int. J. Mol. Sci.*, 16 (2015) 11034-11054.
[25] F. Dashtpeyma, M. Montazerozohori, M. Nasr-Esfahani, Synthesis, characterization, thermal investigation, and antimicrobial activity of some new bis-imine cadmium (II) complexes. *J. Chem. Lett.*, 6 (2025) 142-156.
[26] M.A. Malik, C.K. Jain, G.S. Yadav, S. Kumar, M.S. Khan, M.S. Khan, et al., Heterocyclic Schiff base transition metal complexes in antimicrobial and anticancer chemotherapy. *MedChemComm*, 9 (2018) 409-436.
[27] G. Singh, et al., Synthesis, characterization and UV–visible study of schiff base-acetylene functionalized organosilatrane receptor for the dual detection of Zn2+ and Co2+ ions. *Inorg. Chim. Acta*, 525 (2021) 120465.
[28] T. Fatima, et al., Synthesis, characterization and magnetic studies for a series of compounds having a trinuclear bimetallic Cu2 (II)/Ln (III) system. *Polyhedron*, 186 (2020) 114605.
[29] N.K. Chaudhary, P. Mishra, Spectral Investigation and In Vitro Antibacterial Evaluation of NiII and CuII Complexes of Schiff Base Derived from Amoxicillin and α-Formylthiophene (αft). *J. Chem.*, 2015 (2015) 136285.
[30] M. Kuate, et al., Synthesis, characterization and antimicrobial studies of Co (II), Ni (II), Cu (II) and Zn (II) complexes of (E)-2-(4-dimethylbenzydimino)-glycylglycine,(glygly-DAB) a schiff base derived from 4-dimethylaminobenzaldehyde and glycylglycine. *Int. J. Org. Chem.*, 8 (2018) 298.
[31] B. Bouzerafa, et al., Novel nickel (II) and manganese (III) complexes with bidentate Schiff-base ligand: synthesis, spectral, thermogravimetry, electrochemical and electrocatalytical properties. *Res. Chem. Intermed.*, 42 (2016) 4839-4858.
[32] R. Abdulsattar, B.M. Sarhan, Synthesis and Characterization of Some New Metals Complexes of ((4 Methoxy Benzoyl) Carbamothioyl) Glycine. *Pak. J. Med. Health Sci.*, 16 (2022) 930.
[33] E. Chiyindiko, E.H. Langner, J. Conradie, Spectroscopic behaviour of copper (II) complexes containing 2-hydroxyphenones. *Molecules*, 27 (2022) 6033.
[34] B. Iftikhar, et al., Synthesis, characterization and biological assay of Salicylaldehyde Schiff base Cu (II) complexes and their precursors. *J. Mol. Struct.*, 1155 (2018) 337-348.
[35] A.R. Prasad, A. Joseph, Synthesis, characterization, in silico, and in vitro biological screening of coordination compounds with 1, 2, 4-triazine based biocompatible ligands and selected 3d-metal ions. *Heliyon*, 6 (2020).
[36] F. Ommenya, et al., Synthesis, Characterization and Antibacterial Activity of Schiff Base, 4-Chloro-2-{(E)-[(4-Fluorophenyl) imino] methyl} phenol Metal (II) Complexes. *J. Chem.*, 2020 (2020) 1745236.
[37] G.A. Bain, J.F. Berry, Diamagnetic corrections and Pascal's constants. *J. Chem. Educ.*, 85 (2008) 532.
[38] C.J. Ezeorah, et al., Synthesis, characterization, and in silico studies of 2-[(E)-(2, 5-dimethoxybenzylidene) amino] phenol and 3-[(E)-(2, 5-dimethoxybenzylidene) amino] phenol. *J. Mol. Struct.*, 1270 (2022) 133902.
[39] M. Jisha, C. Isac, Synthesis and characterization of Schiff base complexes of Cu (II), Ni (II), Co (II) complexes of Schiff base derived from furan 3-carboxaldehyde and 3-amino pyridine. *IJSR*, 7 (2017) 10-19.
[40] E.V. Ishaya, et al., Synthesis, characterization, and antimicrobial properties of chromium (III) and iron (III) complexes with schiff base ligands. *J. Chem. Technol.*, 1 (2025) 160-166.
[41] D. Muhammed Aziz, S. Ali Hassan, Synthesis, Characterization, and Evaluation of Tetrazole Derivatives with Pyrrole-2, 5-Dione Moieties as Urease Inhibitors: Exploring Structure-Activity Relationships and Computational Insights. *ChemistrySelect*, 9 (2024) e202401259.
[42] N.R. Babij, et al., NMR chemical shifts of trace impurities: Industrially preferred solvents used in process and green chemistry. *Org. Process Res. Dev.*, 20 (2016) 661-667.
[43] W. Al Zoubi, et al., Synthesis, characterization, and biological activity of Schiff bases metal complexes. *J. Phys. Org. Chem.*, 31 (2018) e3752.
[44] S.J. Hoseyni, M. Manoochehri, M. Daghighi Asli, A novel copper (II) Schiff base complex: synthesis, characterization, and antibacterial activity. *Chem. Rev. Lett.*, 5 (2022) 278-285.
[45] H.R. Shahsavari, et al., Cyclometalated platinum (II) complexes of 2, 2′-bipyridine N-oxide containing a 1, 1′-bis (diphenylphosphino) ferrocene ligand: Structural, computational and electrochemical studies. *Dalton Trans.*, 46 (2017) 2013-2022.

[46] F. Iorhuna, A.M. Ayuba, A.T. Nyijime, Comparative study of skimmianine as an adsorptive inhibitor on Al (110) and Fe (111) crystal surface, using DFT and simulation method. *J. Chem. Lett.*, 4 (2023) 148-155.

[47] M. Heidari Nezhad Janjanpour, et al., Study of the ionization potential, electron affinity and HOMO-LUMO gaps in the smal fullerene nanostructures. *Chem. Rev. Lett.*, 1 (2018) 45-48.

[48] F. Najafi, et al., Fullerene (C20) as a Sensor for the Detection of Nordazepam: DFT Simulations. *Chem. Res. Technol.*, 1 (2025) 18-23.

[49] V. Choudhary, et al., DFT calculations on molecular structures, HOMO–LUMO study, reactivity descriptors and spectral analyses of newly synthesized diorganotin (IV) 2-chloridophenylacetohydroxamate complexes. *J. Comput. Chem.*, 40 (2019) 2354-2363.

[50] T. Abbaz, A. Bendjeddou, D. Villemin, Molecular orbital studies (hardness, chemical potential, electro negativity and electrophilicity) of TTFs conjugated between 1, 3-dithiole. *Int. J. Adv. Res. Sci. Eng. Technol.*, 5 (2018) 5150-5161.

[51] R. Omer, et al., Impact of Solvent Polarity on the molecular properties of Dimetridazole. *El-Cezeri*, 9 (2022) 740-747.

[52] I. Chérif, et al., A theoretical and electrochemical impedance spectroscopy study of the adsorption and sensing of selected metal ions by 4-morpholino-7-nitrobenzofuran. *Heliyon*, 10 (2024).

[53] S. Lakshminarayanan, et al., Molecular electrostatic potential (MEP) surface analysis of chemo sensors: An extra supporting hand for strength, selectivity & non-traditional interactions. *J. Photochem. Photobiol.*, 6 (2021) 100022.